Study of the electrochemical oxidation of 4,6-dimethyldibenzothiophene on a BDD electrode employing different techniques

O. Ornelas Dávila[a], L. Lacalle Bergeron[b], M. M. Dávila Jiménez[a,*], I. Sirés[c], E. Brillas[c], A.F. Roig Navarro[b], J. Beltrán Arandes[b], J.V. Sancho Llopis[b]

[a] *Facultad de Ciencias Químicas, Benemérita Universidad Autónoma de Puebla, México*

[b] *Instituto Universitario de Plaguicidas y Aguas (IUPA), Universidad Jaume I, Castellón de la Plana, Spain*

[d] *Laboratori d'Electroquímica dels Materials i del Medi Ambient, Departament de Química Física, Facultat de Química, Universitat de Barcelona, Martí i Franquès 1-11, 08028 Barcelona, Spain*

* Corresponding author, E-mail: mdavila.uap.mx@gmail.com

Abstract

The electrochemical oxidation of 4,6-dimethyldibenzothiophene (4,6-DMDBT) at low concentrations on a BDD anode was investigated in a monophasic acetonitrile (93.5% v/v)–water (6.5% v/v, 0.01 M $LiClO_4$) solution. Two oxidation steps related to the sequential formation of sulfoxide and sulfone derivatives were identified. Kinetic parameters such as the electron transfer coefficient α, the number of electrons n_α involved in the rate-determining step, the total number of electrons n, the reaction rate constant k^0 and the diffusion coefficient D of 4,6-DMDBT for the first transformation were determined by cyclic voltammetry, differential pulse voltammetry (DPV), square wave voltammetry and bulk electrolysis under potentiostatic conditions. The process was bielectronic with α = 0.57, n_α = 1, $k^0 = 7.46 \times 10^{-6}$ cm s^{-1} and $D = 2.30 \times 10^{-6}$ cm^2 s^{-1}. DPV was the most sensitive electroanalytical technique. Using 27 mg L^{-1} of 4,6-DMTDB, DPV allowed determining a conversion of 91% to sulfoxide after 60 min of electrolysis in a BDD/BDD cell at an anodic potential of 1.50 V, with an apparent rate constant of 0.034 min^{-1}. The electrochemical characterization was corroborated via gas chromatography–mass spectrometry and ultra-high performance liquid chromatography coupled to electrospray ionization and quadrupole time-of-flight mass spectrometry, confirming the formation of the sulfoxide in the first step and the sulfone in the second one as main products, alongside a minor proportion of dimers.

Keywords: Boron-doped diamond, 4,6-Dimethyldibenzothiophene, DPV technique, Electrochemical desulfurization, Oxidation products

1. Introduction

Thioethers like dibenzothiophene (DBT) and its alkylated derivatives are undesirable sulfur compounds in crude oil, being 4,6-dimethyldibenzothiophene (4,6-DMDBT) one of the most important markers of fuel quality. DBTs typically behave as recalcitrant sulfur impurities in liquid and fossil fuels [1-3], asphalt cements [4,5] and pesticides [6-8], thereby attracting the attention because of their negative implications for environment and human health. Organosulfur compounds are also present in complex matrices derived from petroleum [9-12], and they are synthesized for use in materials with different technological applications [13,14]. The organosulfur compounds can be oxidized and finally converted into the corresponding sulfoxide, sulfone or sulfide through different routes [13,15-25], which simplifies their removal by physicochemical methods. On many occasions, such oxidative processes are non-selective because they depend on various factors like the chemical structure of the target molecule, the operation conditions, the oxidation power of the method and materials employed, as well as the reaction medium and solvents used.

Among the oxidation methods to transform aromatic sulfur compounds, the electrochemical techniques are of great interest, since they can provide direct information on the degree of oxidation and the mechanism of degradation of target compounds under different conditions. In some cases, selective electrochemical oxidation is favored when the study is carried out in a mixture of solvents. The quantity of water in the organic solvent [26], as well as the applied oxidation potential, have high influence on the selectivity. Using continuous-flow microreactors, the selective electrochemical conversion of a wide variety of thioethers to sulfoxides or sulfones in the presence of water has been shown to be only governed by the applied potential [27]. Nevertheless, these products are more soluble in water, inducing toxicity to marine organisms [28] and even carcinogenicity [29]. Therefore,

the detection and monitoring of sulfoxides and sulfones is critical. Within this context, physical [10,30] and analytical methods [31,32] have been employed, but the electroanalytical techniques are also a good alternative.

Several authors have demonstrated that differential pulse voltammetry (DPV) and square wave voltammetry (SWV) can be successfully employed to identify and quantify sulfur compounds in complex matrices [33-35], as well as to study their effect on biological activity [36] or on asphalts [4]. In these studies, surface-modified carbonaceous electrodes are generally employed, although boron-doped diamond (BDD) electrodes can be utilized alternatively. In fact, this material is the most suitable anode to degrade and mineralize organic pollutants in water [37-39] and, in the last decade, BDD has been frequently utilized in electroanalysis [6,40-42]. The BDD anodes offer several technological advantages, like a wide potential window in aqueous and organic media, low background currents, high chemical stability, resistance to fouling and controllable surface termination [43-45].

Frequently, the oxidation of organosulfur compounds to their corresponding sulfoxides and sulfones occurs via direct electron transfer in the first step, followed by a series of intermediate reactions. These secondary stages can vary depending on the water present in the medium and the analyte concentration, as well as the nature of the electrode, solvent and supporting electrolyte. This has been evidenced in several articles focused on the electrochemical oxidation of aromatic sulfur compounds and their derivatives [46-48]. Binary mixtures tend to be more useful than pure solvents for practical application or better detection. The application of cyclic voltammetry (CV) in pure acetonitrile (ACN) has shown the irreversibility of the oxidation of DBT, 4-methyldibenzothiophene (4-MDBT) and 4,6-DMDBT [46-48], whereas the presence of water in this medium influences the mechanism of the electrochemical oxidation [27,47,49]. The study of the electrochemical oxidation of

4,6-DMDBT as a recalcitrant compound in an organic solvent in the presence of water, as well as the selective electrodesulfurization of diesel via the production of its sulfoxide (4,6-DMDBTO) and sulfone (4,6-DMDBTO$_2$) intermediates is of great interest. To clarify the mechanism involved, it is necessary to characterize the behavior of the sulfoxide during the bulk electrolysis of 4,6-DMDBT using a BDD electrode. Despite its high cost, BDD shows a high reproducibility in the electrochemical response, stability, resistance to corrosion and low surface fouling related to adsorbed oxidation products [49], which justifies its use.

In this work, the kinetics of the electrochemical oxidation of 4,6-DMDBT in pure ACN and ACN–water has been studied by means of SWV, CV and DPV with a BDD anode of high geometric surface area. The latter technique was proven to be more useful to monitor the conversion of low contents (μmol L^{-1}) of the target molecule into its sulfoxide using an excess of water in ACN. Acetonitrile was used as solvent due to its good miscibility with water, 4,6-DMDBT and the supporting electrolyte. Several analytical techniques were employed to monitor the consumption of 4,6-DMDBT and elucidate the oxidation products generated upon electrolysis in a BDD/BDD cell, including high-performance liquid chromatography with UV detection (HPLC-UV), gas chromatography-mass spectrometry (GC-MS), ultra-high-performance liquid chromatography coupled to electrospray ionization and quadrupole time-of-flight mass spectrometry (UHPLC-ESI-Q-TOF-MS). Inductively coupled plasma mass spectrometry (ICP-MS) was also used to study the degree of corrosion of the BDD electrode.

2. Experimental

2.1. Chemicals and reagents

Dibenzothiophene (99% purity), dibenzothiophene sulfone ($DBTO_2$, 97% purity), 4,6-DMDBT (97% purity) and $LiClO_4$ (> 95% purity) were purchased from Sigma Aldrich. Methanol and hexane of chromatographic grade, and ACS/HPLC acetonitrile (ACN) were provided by Burdick & Jackson. Ultrapure water (18.2 MΩ cm) from a Milli-Q system was used to prepare the ACN–water mixtures. For the electrochemical studies, single compound solutions were prepared by dissolving DBT, $DBTO_2$ or 4,6-DMDBT in ACN for 30–45 min under mechanical stirring. Then, the appropriate mass of $LiClO_4$ or volumes of 0.010 M $LiClO_4$ aqueous solution were added as background electrolyte to obtain different ACN/water (0.010 M $LiClO_4$) mixtures. The lithium perchlorate salt was used as supporting electrolyte due to its high solubility, stability and conductivity in both, acetonitrile and water.

2.2. Electrochemical treatments

Electrochemical measurements of DBT, $DBTO_2$, 4,6-DMDBT and bulk electrolysis of 4,6-DMDBT solutions were performed in 20 mL undivided and divided three-electrode cells (with porous glass disk) using an agar-agar salt bridge with 0.5 M $LiClO_4$. The anode and counter electrode were commercial BDD thin films deposited onto niobium mesh substrates, purchased from Condias (Germany) with a geometric area of 7 cm^2 each. A standard calomel electrode (SCE, 3 M KCl) was employed as the reference electrode, and all potentials given in this manuscript are referred to it. The ohmic drop due to excessive solution resistance was compensated by diminishing the distance separating the reference and working electrode and by means of the potentiostat software (*IR* compensation). The electrochemical measurements

were made using an Eco Chemie Autolab PGSTAT 302 potentiostat-galvanostat controlled with GPES 4.9 software. Before starting the electrochemical measurements, the surface of the BDD electrodes was cleaned first with 10% H_2SO_4 and then, with water under ultrasounds. The electrochemical response and stability of BDD were verified by cycling 5 times from –0.50 to +2.70 V vs. SCE at 0.003 V s^{-1} in an optimized monophasic ACN (93.5% v/v)–water (6.5% v/v, 0.01 M $LiClO_4$) solution. The response and stability were verified by recording cyclic voltammograms before and after each experiment.

DBT, $DBTO_2$ and 4,6-DMDBT are poorly soluble in water and confer low conductivity. Therefore, ACN was employed as co-solvent and $LiClO_4$ as the electrolyte. The good solubility of $LiClO_4$ in ACN and in the ACN-H_2O mixture was achieved at concentrations lower than 0.12 M. SWV, CV, DPV and coulometric experiments were carried out at 25 °C.

2.3. Equipment and analytical conditions

The apparatus and analytical procedures for the determination of the oxidation products are described in Supplementary Material: the HPLC-UV analysis is described in the Text S1, the GC-MS analysis in Text S2, the UHPLC-ESI-Q-TOF-MS analysis in Text S3 and the ICP-MS analysis in Text S4.

3. Results and discussion

3.1. Electrochemical oxidation of 4,6-DMDBT in pure ACN and in ACN–water mixtures

The electrochemical oxidation of 4,6-DMDBT was studied by CV and DPV using a BDD electrode in ACN medium (not dried) and in a mixture of ACN and 6.5% (v/v) water, with 0.010 M $LiClO_4$ as supporting electrolyte. Under these working conditions, a resistive behavior was not observed in the voltammetric responses, as corroborated from the similar

data found at higher $LiClO_4$ contents in selected trials. The electrochemical study was performed using low 4,6-DMDBT concentrations between 1.5 and 27 mg L^{-1} and a potential window from -0.50 to 2.75 V. The latter composition of the reaction medium guaranteed the existence of a wide potential window and a good solubility of both, 4,6-DMDBT and $LiClO_4$.

As shown in Fig. 1a (*curve a'*), the cyclic voltammogram recorded with 14 mg L^{-1} 4,6-DMDBT in pure ACN with $LiClO_4$ displayed an irreversible anodic wave showing a peak at 1.642 V. In contrast, when a technique like DPV was employed, the *curve a'* of Fig. 1b was obtained, revealing the presence of a better-defined irreversible peak I with a smaller peak potential (E_p) of 1.564 V, which was accompanied by two shoulders, II and III, with E_p values of 1.949 and 2.375 V, respectively. This behavior can then be associated to successive oxidation reactions involving the product formed during the first step [47]. Fig. S1 highlights that the half-peak potential ($E_{p/2}$) of each peak found in CV matched with the corresponding E_p value in the DPV curve. On the other hand, the high current observed at the beginning of the DPV curve suggests that it may be associated with the protons released during the oxidation process of 4,6-DMDBT, in a similar way to that of DBT [47].

Fig. 2a shows the change in the DPV profile with the concentration of 4,6-DMDBT in the absence of water. A gradual decay of the peak current (I_p) can be observed as the content of the target compound was decreased from 14 to 1.5 mg L^{-1}. The inset panel of this figure shows a linear increase of I_p with the 4,6-DMDBT concentration. It was also found that the shape of the shoulders appearing at potential higher than 1.6 V changed markedly with the presence of water in the ACN matrix, as evidenced in Fig. 2b. As previously reported [47], the presence of an excess of water in acetonitrile affects the rate of the reaction sequence and can change the reaction mechanism from an EC to an ECEC pathway. The gradual addition of water up to 2.64 M to the 0.010 M $LiClO_4$ solution in ACN enhanced the definition of

peak II, with a concomitant decay of the I_p(I) value (see Fig. 2c). This behavior can be attributed to the selective oxidation of 4,6-DMDBT to 4,6-DMDBTO$_2$ (4,6-dimethyldibenzothiophene sulfone) through 4,6-DMDBTO (4,6-dimethyldibenzothiophene sulfoxide) in the presence of water [49], as will be demonstrated below. Based on these results, a DPV curve was recorded in ACN (93.5% v/v)–water (6.5% v/v, 0.010 M $LiClO_4$) matrix, i.e., ensuring a large excess water. Fig. 2d depicts the presence of two well-defined anodic peaks with similar I_p values at E_p(I) = 1.454 V and E_p(II) = 1.880 V using a solution with 14 mg L^{-1} 4,6-DMDBT. Both E_p values were slightly shifted to more positive values when the 4,6-DMDBT content rose from 14 to 27 mg L^{-1}, whereas the I_p(I) and I_p(II) values varied linearly with 4,6-DMDBT concentration (see the inset of Fig. 2d). According to the results shown in Fig. 2a and d and the graphs for peaks I and II in the presence of excess of water shown in their insets, it is possible to consider a moderate transfer of electrons in the activation step.

As will be discussed below, peak I can be attributed to the formation of the sulfoxide, whereas peak II accounts for by the appearance of the sulfone. According to Cottrell and Mann [50], the sulfone is expected to be produced when water is present in higher concentration than the sulfur compound by a sequence of electrochemical and chemical steps (ECEC). Other authors have described the effect of the presence of traces of water in organic solvents during the electrochemical oxidation or reduction of organic compounds [51]. The selective electrochemical oxidations of some thioethers to sulfoxides or sulfones [27], as well as to sulfone ligands [26], using organic-aqueous mixtures have also been reported. However, no previous studies have been focused on the study of the electrochemical oxidation of 4,6-DMDBT (in a concentration range from 1.5 to 27 mg L^{-1}) by DPV and the elucidation of the degradation kinetics, which is described in following subsections.

Worth noting, peaks I and II in ACN (93.5% v/v)–water (6.5% v/v, 0.010 M $LiClO_4$) were also observed by CV, but with much poorer definition than those determined by means of DPV. Preliminary CV and DPV studies using a BBD electrode at concentrations greater than 50 mg L^{-1} (not shown here) show uniquely one broad band. This indicates that the electrochemical response of 4,6-DMDBT employing the aforementioned techniques also depends on its concentration in the reaction medium.

3.2. Analysis of the electrochemical oxidation of 4,6-DMDBT by cyclic voltammetry

Fig. 3a shows the CV responses of 14 mg L^{-1} 4,6-DMDBT in ACN (93.5% v/v)–water (6.5% v/v, 0.010 M $LiClO_4$) solutions using the BDD electrode at scan rate (v) from 0.005 to 0.100 V s^{-1}. As can be seen, the E_p(I) and E_p(II) values became more positive with increasing v. This suggests that, at least, the oxidation process of 4,6-DMDBT involved in peak I is irreversible under mass-transport control. According to the arrangement of the cell electrodes and using *IR* compensation, it can be discarded that the peak potential (E_p (I)) shift is due to the ohmic drop. On the other hand, for greater precision, the peak potentials were determined by calculating the first derivative of the I vs. E data and treating the inflection point as the oxidation peak.

To verify if the oxidation process of 4,6-DMDBT is irreversible under mass transport control, the I_p(I)-$v^{1/2}$ and log I_p(I)-log v plots are represented in the inset of Fig. 3a. A good linearity can be observed for both relationships, with a slope of 0.50 for the second one, in agreement with the theoretical value of a diffusion-controlled process. However, the aforementioned linear fittings did not intercept the origin, which could indicate that the electrode reaction related to peak I was followed by a homogeneous chemical reaction [52,53]. A plot of the scan rate normalized peak current (I_p $v^{-1/2}$) against v can be used as

criterion to determine the nature of the irreversibility of the electrode process [52]. In the case of 14 mg L^{-1} 4,6-DMDBT, the shape of this plot is shown in Fig. S2. The irreversibility of peak I could then be plausibly associated to the existence of a coupled homogeneous chemical reaction [47], probably involving the water present in the matrix, following the initial electrochemical reaction.

To better understand the first step involving heterogeneous charge transfer, the factor αn_α for the process related to peak I, where α is the transfer coefficient and n_α is the number of electrons involved in the rate-determining-step, was evaluated. A first approach was made by plotting the current-voltage curve (subtracting the background current) from an anodic polarization at a low scan rate (0.005 V s^{-1}), as shown in Fig. 3b. The inset of this figure highlights a slope of 0.103 V dec^{-1}. Taking into account that the theoretical value for this slope is b = $2.3RT/\alpha n_\alpha F$, an $\alpha n_\alpha = 0.57$ was estimated. This value suggests a one-electron transfer in the rate-determining step. On the other hand, the αn_α value was also estimated from Eq. (1), established for an irreversible charge transfer process [53]:

$$E_p - E_{\frac{p}{2}} = \frac{1.857RT}{\alpha n_\alpha F} \quad (1)$$

where E_p and $E_{p/2}$ are the peak and half-peak potentials determined for peak I by CV. The average (E_p-$E_{p/2}$) value was 0.076 V over the scan range from 0.01 to 0.100 V s^{-1}, yielding $\alpha n_\alpha = 0.63$ from Eq. (1). Therefore, the results obtained for αn_α by these two methods are in good agreement, confirming that a one-electron transfer is the rate-limiting step in the oxidation of 4,6-DMDBT on BDD, with $\alpha = 0.5$ [53,54].

3.3. Determination of E^0, k^0 and D

A plot of the peak potential, E_p with the logarithm of the scan rate, ν is shown in Fig. S3a. This plot demonstrates a good linearity for irreversible oxidation process 4,6-DMDBT and can be fitted with the following equation [55]:

$$E_p = E^0 + \frac{RT}{2\alpha n_\alpha F}\, x\, \left[0.78 + 1.15\, x \log\left(\frac{\alpha n_\alpha F D}{k^2 RT}\right)\right] + 1.15\, x\, \frac{RT}{\alpha n_\alpha F}\, x\, log v \qquad (2)$$

where E^0 is the standard electrode potential, α is the transfer coefficient, n_α is the number of electrons involved in the rate-determining step, αn_α is the overall electron transfer coefficient, l, v is the scan rate, and k is the standard heterogeneous rate constant of the reaction, having the other symbols their usual meaning. Thus, the αn_α-value can be calculated from the slope of E_p vs. log v for peak I, as presented in Fig. S3a. From Eq. (2), a linear relationship between E_p and v was obtained, as depicted in Fig. S3b, giving rise to E^0 = 1.6018 V by extrapolating the ordinate to v = 0. Using this E^0 value and converting Eq. (2) into Eq. (3) at log v = 0, a value of $k^0 = 7.46 \times 10^{-6}$ cm s^{-1} was determined:

$$1.8342 = 1.4789 + \frac{RT}{2\alpha n_\alpha F}\left[0.78 + 1.15 log\left(\frac{\alpha n_\alpha F D}{k^2 RT}\right)\right] \qquad (3)$$

The diffusion coefficient for 4,6-DMDBT at 14 mg L^{-1} in ACN (93.5% v/v)–water (6.5% v/v, 0.010 M $LiClO_4$) was then estimated from the linear dependence of I_p vs. $v^{1/2}$, given in the inset of Fig. 3a, according to the Randles-Sevcik equation [53]:

$$I_p = 2.99x10^5 n(\alpha n_\alpha)^{\frac{1}{2}} C_0 A D^{\frac{1}{2}} v^{\frac{1}{2}} \qquad (4)$$

where A is the electrode surface area, D is the diffusion coefficient, and C_0 is the bulk concentration of 4,6-DMDBT. From Eq. (4), a D value of 2.3×10^{-6} cm^2 s^{-1} for this substrate

256 was obtained. Note that using DPV (see below), a very close value of $D = 3.1 \times 10^{-6}$ cm^2 s^{-1}
257 was calculated.

258 The diffusion coefficient was also estimated by using a linear correlation between the
259 diffusion coefficient and molecular weight according to a semi-empirical equation [56]:

260 $$D_i = 1.236x10^{-11}\frac{T}{\eta}\left(4 - \frac{M_{\mathrm{wi}}}{135.4}\right) \quad (5)$$

261 where M_{wi} is the molecular weight of species i, η is the medium viscosity in Poises and T the
262 is the absolute temperature. A diffusion coefficient of 2.4×10^{-6} cm^2 s^{-1} was calculated, a
263 value similar to that obtained experimentally.

264 The chronoamperometry method was also used to determine the diffusion coefficient D.
265 As can be seen in Fig. S4, the plot of j_p vs. the $t^{-1/2}$ showed a linear relationship for two
266 concentrations 4,6-DMDBT (14 and 27 mg L^{-1}). Using the obtained slopes and the Cottrell
267 equation (6) at such concentrations [53], where C_O is the bulk concentration and A_g is the
268 geometric area of the BDD electrode, a D value of 1.74×10^{-6} cm^2 s^{-1} was determined,
269 which is similar to the values mentioned above. Note that using DPV (see below), a very
270 close value of $D = 2.2 \times 10^{-6}$ cm^2 s^{-1} was found.

271 $$I = nFA_gD^{1/2}C_0\Pi^{-1/2}t^{-1/2} \quad (6)$$

272 *3.4. Analysis of the electrochemical oxidation of 4,6-DMDBT by differential pulse*
273 *voltammetry*

274 The electro-oxidation of 4,6-DMDBT in ACN (93.5% v/v)–water (6.5% v/v, 0.010 M
275 $LiClO_4$) was also investigated at different scan rates and substrate concentrations using the
276 DPV technique, in order to verify the kinetic parameters previously calculated by CV. The
277 curves obtained are shown in Fig. 4a and b, respectively. Fig.4a presents a dependence of I

with v similar to that described by CV in Fig. 3a, whereas Fig. 4b evidences a linear increase of I_p of peak I with the substrate concentration from 7 to 92 µM, as shown in its inset panel. When DPV was applied, the ratio of faradaic to capacitive current became large, which allows explaining the improved definition and resolution of the oxidation peaks in pure ACN medium (see Fig. 1b) and in the mixed matrix (see Fig. 2b and d). Hence, aiming to clarify if the oxidation process of 4,6-DMDBT really presented a coupled chemical reaction, the (I_p $v^{-1/2}$) vs. v plot was obtained from the data of Fig. 4a. Fig. S5a and b highlight a clear exponential decay of that factor for peaks I and II, respectively with increasing v. As stated above, this behavior is consistent with an EC mechanism, corroborating that each heterogeneous electron transfer of peaks I and II was followed by an irreversible homogeneous chemical reaction. Moreover, the inset of Fig. 4a shows a slope of 0.2123 for the linear dependence of log I_p on log v, confirming that the process was controlled by diffusion. However, the low value of this slope as compared to 0.5 obtained by CV (see the inset of Fig. 3a) suggests a weak adsorption of the electroactive species on the electrode.

The data of Fig. 4b at each concentration were employed to determine a mean value of 0.160 V for the width of the peak I at its half height ($W_{1/2}$). Then, from Eq. (7), established for an irreversible electrochemical reaction [57], an apparent $\alpha n = 0.56$ was obtained.

$$W_{1/2} = \frac{0.090}{\alpha n} \quad (7)$$

The value of the apparent diffusion coefficient was verified using Eq. (8), which relates the I_p of peak I in DPV analysis with the given concentration C_0 of the electroactive 4,6-DMDBT in the solution [58]:

$$I_p = \frac{nAFD^{\frac{1}{2}}C_0}{\pi t_m^{\frac{1}{2}}}\left(\frac{1-\sigma}{1+\sigma}\right) \quad (8)$$

where t_m represents the modulation time (in *s*) and the parameter σ for an irreversible electrochemical reaction is given by the following expression [59]:

$$\sigma = \exp\left(\frac{\alpha n_\alpha F \Delta E}{2RT}\right) \quad (9)$$

where ΔE is the modulation amplitude (in V). From the results of Fig. 4b, an apparent D value of 2.17×10^{-6} cm^2 s^{-1} was calculated, in good agreement with $D = 2.43 \times 10^{-6}$ cm^2 s^{-1} obtained from the CV results commented above.

The total number of electrons (n) involved in peak I was estimated from Eq. (4). Considering $\alpha n_\alpha = 0.57$, $C_0 = 6.59 \times 10^{-8}$ mol cm^{-3} (i.e., the concentration of 4,6-DMDBT in solution), $A = 7$ cm^2 and $D^{1/2} = 1.47 \times 10^{-3}$ cm s$^{-1/2}$ (calculated from the DPV data), $n = 1.88$ was found. On the other hand, the n electrons related to the oxidation reaction of 20 mL of 27 mg L^{-1} 4,6-DMDBT in ACN (93.5% v/v)–water (6.5% v/v, 0.010 M $LiClO_4$) were also obtained by electrolysis in a BDD/BDD cell at an anodic potential (E_{an}) of 1.50 V for 60 min. The total charge consumed during the electrolysis (Q_t) was obtained from the experimental *I-t* plot, which is related to the *n*-value as follows:

$$Q_t = nFN \quad (10)$$

where F is the Faraday constant and N is the number of moles of substrate. From this assay, the coulometric *n*-value was 2.09, corroborating that it is a bielectronic process as proposed in the literature [47]. As recently published, the electrochemical oxidation of methylated dibenzothiophenes is a process that involves several steps of charge transfer and ECEC with coupled chemical reactions [47], when an excess of water in the acetonitrile matrix is present. However, in the different EC steps the formation of dimers may be involved (as will be shown

321 later) and hence, so the proposal of a mechanism is very complex. Therefore, it is important
322 to point out that the kinetic parameters described above are average values, since they were
323 evaluated considering a simple diffusion model. A more appropriate model for the
324 experimental system used in this work should consider a two-step diffusion mechanism,
325 which is beyond the scope of the present work.

326 *3.5. Proposed reaction pathway*

327 From the above results, a plausible pathway for 4,6-DMDBT oxidation within the
328 potential range from 1.35-2.70 V is proposed in Fig 5. The large presence of water
329 (approximately 3.6 M at the 6.5% v/v content) in ACN favored the hydrolysis of the radical
330 cation initially formed from a one-electron oxidation, being the rate-determining step of stage
331 I. The resulting species then evolved to the sulfoxide 4,6-DMDBTO via another one-electron
332 oxidation and two deprotonation steps. Overall, the transformation of 4,6-DMDBT into 4,6-
333 DMDBTO involved the addition of one water molecule and the loss of two electrons and two
334 protons, occurring at E = 1.5 V. A similar process can be envisaged for the electrochemical
335 oxidation of 4,6-DMDBTO to the sulfone 4,6-DMDBTO$_2$ via two electrons in the process II.
336 It is also shown in Fig. 5 that, when E > 1.7 V was applied, 4,6-DMDBT was directly
337 transformed into 4,6-DMDBTO$_2$ with the participation of two water molecules and the
338 exchange of four electrons and release of four protons. At high anode potentials (E > 1.7 V),
339 the participation of oxidizing species [O], like hydroxyl radical, generated upon electrolysis
340 of water cannot be discarded either in the oxidative process [49].

3.6. DPV and SWV analysis of the products formed during the oxidation of 4,6-DMDBT

According to the CV profiles shown in Fig. 1 and 3, no reduction peak was observed during the backward scan. The absence of a cathodic peak suggests that the by-products of the oxidation of 4,6-DMDBT evolve into stable end products, which are not susceptible to be reduced during the cathodic scan by this technique. Therefore, it is interesting to use DPV and SWV to study the reactivity and electrochemical stability of the final products immediately after their generation under our working conditions.

The anodic and subsequent cathodic DPV curves recorded with 14 mg L^{-1} 4,6-DMDBT in ACN (93.5% v/v)–water (6.5% v/v, 0.010 M $LiClO_4$) within the potential range from -0.50 to 1.75 V and -0.50 to 2.60 V are presented in Fig. S6a and S6b, respectively. Cathodic peaks (*curves b´*) related to the respective oxidation peaks I and II, with similar I_p and E_p values *(curves a´*), can be observed in both figures. These results suggest that in the first anodic scan, the sulfoxide and/or sulfone products from 4,6-DMDBT oxidation were generated near the electrode surface and then, consumed during the cathodic sweep. One can assume that the release of the products from the interface was slow and, consequently, they could be easily reduced. This means that the products were stable when generated and did not disappear from the electrical double layer, thereby favoring their reduction.

The anodic and cathodic DPV responses of 4,6-DMDBT were then compared with those of 27 mg L^{-1} of standard DBT and $DBTO_2$ under the same experimental conditions. As shown in the *curve a'* of Fig. S7a, the anodic scan for DBT showed peaks I and II similar to those of 4,6-DMDBT; the peak II appeared at a potential around 2.0 V, very close to that obtained for $DBTO_2$ (see *curve b'* of Fig. S7a). Fig. S7b depicts both, the anodic and cathodic peaks with the same E_p = 2.12 V, obtained for the DPV analysis of $DBTO_2$, in an analogous way

364 to that of peak II of 4,6-DMDBT (see Fig. S6b). This allows considering that the peak II
365 appearing during the oxidation of DBT or 4,6-DMDBT can be attributed to the oxidation of
366 the corresponding sulfoxide to sulfone. This was corroborated by chromatographic analysis
367 of the 4,6-DMDBT oxidation products, as will be discussed below.

368 The square wave voltammograms obtained for 14 mg L^{-1} 4,6-DMDBT in Fig. S8a and
369 b showed similar results to those of DPV in Fig. S6a and S6b.

370 *3.7. Kinetic analysis of 4,6-DMDBT removal by differential pulse voltammetry*

371 The decay of the 4,6-DMDBT concentration in an ACN (93.5% v/v)–water (6.5% v/v,
372 0.010 M $LiClO_4$) solution containing 27 mg L^{-1} was monitored by DPV analysis of samples
373 collected during its bulk oxidation using a BDD/BDD cell at E_{an} = 1.50 V, aiming to know
374 the optimum electrolysis time for the formation of the sulfoxide. Fig. 6a and b present the
375 evolution of the DPV curves at short and long electrolysis times, respectively. As expected,
376 the highest I_p for peak I within the potential range 1.20-1.70 V was reached for the initial
377 solution. This peak corresponded to the oxidation of 4,6-DMDBT to its sulfoxide 4,6-
378 DMDBTO. At E > 1.70 V, the subsequent conversion to the sulfone 4,6-$DMDBTO_2$ took
379 place.

380 Fig. 6a and b disclose a rapid decrease of the height of peak I due to the progressive
381 removal of 4,6-DMDBT with formation of its main product 4,6-DMDBTO. The inset panels
382 of both figures highlight the decrease of I_p(I) as the electrolysis was prolonged, achieving its
383 total disappearance at 60 min, time at which peak I was not detected any more. The I_p(II)
384 value can then be used to monitor the stability of the sulfoxide. The inset panels of Fig. 6a
385 and b also inform about a gradual drop of I_p(II) after 90 min of electrolysis. For example, this
386 peak current underwent a reduction of 41% after 240 min of electrolysis, suggesting again

that the sulfone was originated via the sulfoxide as intermediate. Two reasons could explain this trend. First, by fixing an E_{an} = 1.50 V, the potential difference between the two BDD electrodes was around 1.85 V. At this potential, a certain oxidation of the produced 4,6-DMDBTO$_2$ could occur, thus causing the decay of I_p(II). A second possibility could be the occurrence of a certain coating of the electroactive sites of the BDD anode by residual oxidation products as the electrolysis progressed, inhibiting the diffusion of 4,6-DMDBTO from the solution to the anode.

The 4,6-DMDBT concentration was quantified using a calibrated I_p(I)–C plot, which became linear within a substrate range between 0.75 and 27 mg L^{-1}. The corresponding equation was $I_p(I) = 0.8043 + 0.7100C$, with a squared regression coefficient (R^2) of 0.993. The conversion of 4,6-DMDBT into 4,6-DMDBTO for 60 min at E_{an} = 1.50 V was 91%, being determined as follows:

$$\%\ \text{Conversion} = \left(\frac{C_0 - C_t}{C_0}\right) x100 \qquad (11)$$

It was also found that the concentration decay obeyed a pseudo-first-order kinetics, with an apparent rate constant (k) of 0.034 min^{-1} (R^2 = 0.983) as the slope of ln (C_0/C) vs. t.

3.8. Kinetic analysis of 4,6-DMDBT removal by HPLC-UV

The concentration decay for the same trial described in the previous subsection was also monitored by HPLC with an UV/Vis detector set at λ = 232 nm. Fig. 7a shows the total ion chromatogram recorded at different electrolysis times. Two main peaks with retention time (t_R) of 5.55 and 10.81 min were clearly distinguished. The intensity of the latter peak decreased at longer time, in agreement with the abatement of 4,6-DMDBT, whereas the

intensity of the former peak increased progressively due to the continuous production of 4,6-DMDBTO.

The 4,6-DMDBT concentration was quantified by using the calibration curve (Intensity = 0.6781 + 24.4687*C*), with R^2 = 0.998. Fig. 7b presents the percentage of conversion of the substrate into the sulfoxide calculated from Eq. (11), along with the good pseudo-first-order reaction kinetics found for the concentration abatement. A conversion of 91% was determined after 90 min of electrolysis and an apparent *k*-value of 0.025 min^{-1} (R^2 = 0.993) was obtained, being close to 0.034 min^{-1} found by DPV. Some authors attempted the catalytic oxidation of 4,6-DMDBT following different procedures at ambient temperature [60,61], reporting *k*-values of about one to four magnitude orders smaller than the value found in this work via electrochemical oxidation. In contrast, Jin et al., [22] employed a molybdenum oxide catalyst loaded on mesoporous alumina, obtaining much greater *k*-values around 0.236 min^{-1}, although they worked at higher temperatures ranging between 45 and 55 ºC.

3.9. Kinetic analysis of 4,6-DMDBT removal by GC-MS

The solutions collected at different times upon electrolysis of solutions containing 27 mg L^{-1} 4,6-DMDBT in ACN (93.5% v/v)–water (6.5% v/v, 0.010 M $LiClO_4$) using the BDD/BDD cell at E_{an} = 1.50 V were analyzed by GC-MS. In Fig. 8a, the total ion chromatograms recorded at increasing electrolysis times are compared. Before electrolysis, the peak 1 at t_R = 17.47 min (plot *a'*) with *m/z* 212 corresponded to the target molecule, 4,6-DMDBT (see Fig. 8b). After 15 min of electrolysis (plot *b'*), its peak intensity decreased and a new peak 2 appeared at t_R = 20.24 min with *m/z* 228. As expected and according to the mass spectrum of Fig. 8c, this product was identified as the sulfoxide, 4,6-DMDBTO. Fig. 8a also shows that, at longer electrolysis time, the intensity and area of peak 1 decreased,

whereas those of peak 2 increased (plot *c'*). After 60 min of electrolysis, peak 1 disappeared completely (plot *d'*), in good agreement with the time needed for total 4,6-DMDBT removal found by DPV. From an accurate analysis of the area under the peaks of the total chromatograms, one can deduce a maximum formation of the sulfoxide from the oxidation of 4,6-DMDBT after 45 min of electrolysis (see Fig. 8a). After that time, the intensity and area of peak 2 slowly dropped down. This behavior is consistent with that observed during the monitoring of the electrochemical oxidation of 4,6-DMDBT by DPV and HPLC-UV. Therefore, the results of the kinetic studies by DPV, HPLC-UV-Vis and GC-MS, evaluating the consumption of 4,6-DMDBT during its oxidation to form the main oxidation products, showed that it is unnecessary to regenerate the BDD surface after each electrochemical characterization and electrolytic trial. This corroborates the great stability and resistance to fouling of this anode.

3.10. UHPLC-ESI-Q-TOF-MS analysis of the oxidation products and anode stability

The study described above confirmed the formation of 4,6-DMDBTO and 4,6-DMDBTO$_2$ from the electrochemical oxidation of 4,6-DMDBT. The UHPLC-ESI-Q-TOF-MS analysis of the electrolyzed extracts in divided and undivided cells indicated the formation of other products as a result of the electrochemical oxidation process. The total ion chromatogram of Fig. S9 obtained after bulk electrolysis of solutions containing 27 mg L^{-1} 4,6-DMDBT in undivided and divided cells during 90 min at E_{an} = 1.50 V shows a strong peak at t_R = 8.34 min (P5) and 5 smaller peaks at t_R = 6.03 min (P1), 7.02 min (P2), t_R = 7.84 min (P3), t_R = 8.05 min P4) and t_R = 9.96 min (P6). Low collision energy (LE) and high collision energy (HE) mass spectra alongside mass fragments are shown in Fig. S10-S16 and Table S1. These LE and HE mass spectra confirm that the predominant anodic oxidation

product corresponds to 4,6-DMDBTO (compound P5, Fig. S14). This agrees with the reaction mechanism proposed in Fig. 5. The second important anodic oxidation product according to Fig. S9 is the dimer of 4,6-DMDBT (compound P6, Fig. S15). The electrochemical dimerization process of different aromatic compounds at a platinum electrode has been reported [62,63], as well as the spectral behavior of the radical cations of dibenzothiophene and some of its derivatives by electron paramagnetic resonance [64]. On the other hand, according to the LE and HE mass spectra (Fig. S11), the product P2 corresponds to the oxidation of 4,6-DMDBT, which can in turn involve two or more successive reactions. In contrast, the products P3, P4 and P7 are produced from the oxidation of dimer 4,6-DMDBT (Fig. S12, S13 and S16, respectively). Fig. 9 presents the proposed schematic route for the formation of these compounds.

The UHPLC-ESI-Q-TOF-MS analysis of the extracts obtained after electrolysis times longer than 90 min and E_{an} of 1.5 and 2.0 V from solution with 27 mg L^{-1} 4,6-DMDBT (Fig. S17) showed a practical consumption of the products P1-P4, P6 and P7. The total ion chromatogram of Fig. S17a obtained after bulk electrolysis at E_{an} = 1.50 V depicts a strong peak 1 at t_R = 8.30 min and a second smaller peak 2 at t_R = 8.43 min. When the electrolysis was performed at E_{an} = 2.00 V, the presence of only one main peak 2 at t_R = 8.43 min, in a larger proportion than that of peak obtained at E_{an} = 1.50 V, was found (Fig. S17b). No other peaks were observed, meaning that no intermediates were formed or they were degraded under the analysis conditions. The LE and HE mass spectra shown in Fig. S17a' and b′, respectively, confirm that the most relevant anodic oxidation products were 4,6- DMDBTO (compound 1, t_R = 8.30 min) and 4,6-DMDBTO$_2$ (compound 2, t_R = 8.43 min). This agrees with the reaction mechanism proposed in Fig. 5.

An essential parameter in practice to electrolyze 4,6-DMDBT in ACN–water solutions with $LiClO_4$ as supporting electrolyte is the anode stability. The application of an electric field may originate mini-cracks in the BDD thin film, allowing the penetration of the solution and its possible interaction with the substrate, with the consequent release of Nb ions to the medium. Such corrosion phenomenon would cause a strong reduction of the service life of the BDD electrode, with a negative impact on the type of electrochemical oxidation processes considered in this work. To confirm the extent of this damage, the final electrolyzed solutions of 4,6-DMDBT at E_{an} values of 1.50 and 2.00 V were analyzed by ICP-MS and, worth mentioning, no Nb was detected. This indicates that the anodic dissolution of the Nb support did not occur and hence, the BDD anode is a suitable material to operate under the conditions described in the present work.

4. Conclusions

CV and DPV analyses showed that the electrochemical oxidation of 4,6-DMDBT on a BDD electrode in aqueous acetonitrile with $LiClO_4$ as supporting electrolyte occurs through two consecutive bielectronic processes. A transfer coefficient of 0.57 was determined for the first oxidation step in the potential range 1.25-1.75 V, with one electron transferred in the rate-determining step. The diffusion coefficient of the target compound was found to be 2.3 $\times 10^{-6}$ cm^2 s^{-1} by CV, very close to 2.2 $\times 10^{-6}$ cm^2 s^{-1} derived from DPV analysis. About 91% conversion of 4,6-DMDBT, following a pseudo-first-order kinetic decay with an apparent rate constant of 0.034 min^{-1}, was determined by DPV after 60 min of electrolysis in a BDD/BDD cell at E_{an} = 1.50 V. The GC-MS technique allowed confirming the presence of the corresponding sulfoxide 4,6-DMDBTO as the main product in the first step. UHPLC-

ESI-Q-TOF-MS analysis of the extracts obtained from the electrolyzed solutions confirmed the production of the sulfoxide 4,6-DMDBTO, which was transformed into sulfone 4,6-$DMDBTO_2$ in the second step. The use of BDD anode and suitable electrochemical and chromatographic techniques allowed the selective conversion of 4,6-DMDBT and the full characterization of the process.

Acknowledgments

O. Ornelas is grateful for the postdoctoral scholarship (PRODEP) No. DSA/103.5/16/14302 and VIEP-BUAP-00654. This work was funded by the Benemérita Universidad Autónoma de Puebla (VIEP-BUAP) and by SEP-DGESU. Current address: We thank Patricia Ruíz Gutiérrez and Lab. Adsorption (ICUAP, Puebla, Mexico) for performing the LC-DAD analysis and for access to the apparatus, respectively.

References

[1] C. Song, X. Ma, New design approaches to ultra-clean diesel fuels by deep desulfurization and deep dearomatization, Appl. Catal. B: Environ. 41 (2003) 207–238. Doi: 10.1016/S0926-3373(02)00212-6

[2] T. Schade, J.T. Andersson, Speciation of alkylated dibenzothiophenes in a deeply desulfurized diesel fuel, Energy Fuels 20 (2006) 1614–1620. Doi: 10.1021/ef0502507

[3] N.K. Bordoloi, S.K. Rai, M.K. Chaudhuri, A.K. Mukherjee, Deep-desulfurization of dibenzothiophene and its derivatives present in diesel oil by a newly isolated bacterium *Achromobacter* sp. to reduce the environmental pollution from fossil fuel combustion, Fuel Process. Technol. 119 (2014) 236–244. Doi: 10.1016/j.fuproc.2013.10.014

[4] G.D. da Silveira, L.M. de Carvalho, N. Montoya, A. Domenech-Carbó, Solid state electrochemical behavior of organosulfur compounds, J. Electroanal. Chem. 806 (2014) 180–190. Doi: 10.1016/j.jelechem.2017.10.055

[5] G.D. da Silveira, C.K. Hoinacki, R.B. Goularte, P.C. Do Nascimento, D. Bohrer, M. Cravo, L.F.M. Leite, L.M. de Carvalho, A cleanup method using solid phase extraction for the determination of organosulfur compounds in petroleum asphalt cements, Fuel. 202 (2017) 206–215. Doi: 10.1016/j.fuel.2017.04.020

[6] D. Hainzl, L.M. Cole, J.E. Casida, Mechanisms for selective toxicity of fipronil insecticide and its sulfone metabolite and desulfinyl photoproduct, Chem. Res. Toxicol. 11 (1998) 1529–1535. Doi: 10.1021/tx980157t

[7] M.C. Henderson, S.K. Krueger, L.K. Siddens, J.F. Stevens, D.E. Williams, S-Oxygenation of the thioether organophosphate insecticides phorate and disulfoton by human lung flavin-containing monooxygenase 2, Biochem. Pharmacol. 68 (2004) 959–967. Doi: 10.1016/j.bcp.2004.05.051

[8] J. Chýlcová, M. Tomáškova, I. Švancara, L. Janíková, R. Šelešovská, Determination of methiocarb pesticide using differential pulse voltammetry with a boron-doped diamond electrode, J. Anal. Methods 7 (2015) 4671–4677. Doi: 10.1039/C5AY00979K

[9] G. Gryglewicz, P. Rutkowski, J. Yperman, Characterization of sulfur compounds in supercritical coal extracts by gas chromatography-mass spectrometry, Fuel Process. Technol. 77-78 (2002) 167–172. Doi: 10.1016/S0378-3820(02)00046-2

[10] J. Rankin, K. Litz, S. Briggs, T. McCaskill, M. Scudder, S. Khalid, R. Budhani, Selective desulfonylation of oxidized sulfur compounds in crude oil by alcohol-

543 mediated nucleophilic attack studied by XANES and XRF spectroscopy, Preprints
544 (2016) 1–8. Doi: 10.20944/preprints201609.0075.v1
545 [11] O.O. Sadare, F. Obazu, M.O. Daramola, Biodesulfurization of petroleum distillates -
546 Current status, opportunities and future challenges, Environments 4 (2017) 85. Doi:
547 10.3390/environments4040085
548 [12] P. Li, D. Hu, D. Xie, J. Chen, L. Jin, B. Song, Design, synthesis, and evaluation of new
549 sulfone derivatives containing a 1,3,4-oxadiazole moiety as active antibacterial agents,
550 J. Agric. Food Chem. 66 (2018) 3093–3100. Doi: 10.1021/acs.jafc.7b06061
551 [13] R.V. Kupwade, A concise review on synthesis of sulfoxides and sulfones with special
552 reference to oxidation of sulfides, J. Chem. Rev. 1 (2019) 99–113. Doi:
553 10.33945/SAMI/JCR.2019.1.99113
554 [14] S. Matavos-Aramyan, S. Soukhakian, M.H. Jazebizadeh, Selected methods for the
555 synthesis of sulfoxides and sulfones with emphasis on oxidative protocols, Phosphorus,
556 Sulfur, Silicon Relat. Elem. 195 (2020) 181–193. Doi:
557 10.1080/10426507.2019.1672691
558 [15] Y. Shiraishi, Y. Taki, T. Hirai, I. Komasawa, A novel desulfurization process for fuel
559 oils based on the formation and subsequent precipitation of S-alkylsulfonium salts. 1.
560 Light oil feedstocks, Ind. Eng. Chem. Res. 40 (2001) 1213–1224. Doi:
561 10.1021/ie001090j
562 [16] Y. Che, W. Ma, Y. Ren, C. Chen, X. Zhang, J. Zhao, Photooxidation of
563 dibenzothiophene and 4,6-dimethyldibenzothiophene sensitized by N-
564 methylquinolinium tetrafluoborate: mechanism and intermediates investigation, J.
565 Phys. Chem. B. 109 (2005) 8270–8276. Doi: 10.1021/jp0441238

[17] M.A. Gondal, H.M. Masoudi, J. Pola, Laser photo-oxidative degradation of 4,6-dimethyldibenzothiophene, Chemosphere 71 (2008) 1765–1768. Doi: 10.1016/j.chemosphere.2008.01.035

[18] D.P. Morales, A.S. Taylor, S.C. Farmer, Desulfurization of dibenzothiophene and oxidized dibenzothiophene ring systems, Molecules 15 (2010) 1265–1269. Doi: 10.3390/molecules15031265

[19] R. Sundararaman, X. Ma, C. Song, Oxidative desulfurization of jet and diesel fuels using hydroperoxide generated in situ by catalytic air oxidation, Ind. Eng. Chem. Res. 49 (2010) 5561–5568. Doi: 10.1021/ie901812r

[20] H.X. Zhang, J.J. Gao, H. Meng, Y.Z. Lu, C.X. Li, Catalytic oxidative desulfurization of fuel by H_2O_2 in situ produced via oxidation of 2-propanol, Ind. Eng. Chem. Res. 51 (2012) 4868−4874. Doi: 10.1021/ie300035c

[21] T.A. Saleh, Applying nanotechnology to the desulfurization process in petroleum engineering, IGI Global 2016. Doi: 10.4018/978-1-4666-9545-0

[22] W. Jin. Y. Tian, G. Wang, D. Zeng, Q. Xu, J. Cui, Ultra-deep oxidative desulfurization of fuel with H_2O_2 catalyzed by molybdenum oxide supported on alumina modified by Ca^{2+}, RSC Adv. 7 (2017) 48208–48213. Doi: 10.1039/C7RA08900G

[23] O. Senko, O. Maslova, M. Gladchenko, S. Gaydamaka, A. Akopyan, S. Lysenko, E. Karakhanov, E. Efremenko, Prospective approach to the anaerobic bioconversion of benzo- and dibenzothiophene sulfones to sulfide, Molecules 24 (2019) 1736. Doi: 10.3390%2Fmolecules24091736

[24] X. Ma, Y. Liu, L. Du, J. Zhou, I.E. Markó, Post-functionalization of dibenzothiophene to functionalized biphenyls via a photoinduced thia-Baeyer-Villiger oxidation, Nat. Commun. 11 (2020) 914. Doi: 10.1038/s41467-020-14522-7.

590 [25] C.A. Ortega Ramirez, A. Kwan, Q.X. Li, Rhamnolipids induced by glycerol enhance
591 dibenzothiophene biodegradation in *Burkholderia* sp. C3, Engineering 6 (2020) 533–
592 540. Doi: 10.1016/j.eng.2020.01.006
593 [26] A. de León, J. García-Antón, J. Ros, G. Guirado, I. Gallardo, J. Pons, Environmentally
594 benign and selective synthesis of hybrid pyrazole sulfoxide and sulfone ligands, New
595 J. Chem. 37 (2013) 1889–1894. Doi: 10.1039/C3NJ00161J
596 [27] G. Laudadio, N.J.W. Straathof, M.D. Lanting, B. Knoops, V. Hessel, T. Noël, An
597 environmentally benign and selective electrochemical oxidation of sulfides and thiols
598 in a continuous-flow microreactor, Green Chem. 19 (2017) 4061–4066. Doi:
599 10.1039/C7GC01973D
600 [28] F. Berthou, V. Vignier, Analysis and fate of dibenzothiophene derivatives in the marine
601 environment, Int. J. Environ. Anal. Chem. 21 (1986) 81–96. Doi:
602 10.1080/03067318608078392
603 [29] D.T. Seymour, A.G. Verbeek, S.E. Hrudey, P.M. Fedorak, Acute toxicity and aqueous
604 solubility of some condensed thiophenes and their microbial metabolites, Environ.
605 Toxicol. Chem. 16 (1997) 658–665. Doi: 10.1002/etc.5620160409
606 [30] O.E. Eremina, A.V. Sidorov, T.N. Shekhovtsova, E.A. Goodilin, I.A. Veselova, Novel
607 multilayer nanostructured materials for recognition of polycyclic aromatic sulfur
608 pollutants and express analysis of fuel quality and environmental health by surface
609 enhanced Raman spectroscopy, ACS Appl. Mater. Interfaces 9 (2017) 15058−15067.
610 Doi: 10.1021/acsami.7b02018
611 [31] F. Traulsen, J.T. Andersson, M.G. Ehrhardt, Acidic and non-acidic products from the
612 photo-oxidation of the crude oil component dibenzothiophene dissolved in seawater,
613 Anal. Chim. Acta 392 (1999) 19–28. Doi: 10.1016/S0003-2670(99)00055-0

614 [32] W.E. Rudzinski, Y. Zhang, X. Luo, Mass spectrometry of polyaromatic sulfur
615 compounds in the presence of palladium(II), J. Mass Spectrom. 38 (2003) 167–173.
616 Doi: 10.1002/jms.426
617 [33] Y. Yurum, H. Ozyoruk, N. Altuntag, H. Gulce. Identification of organic sulfur
618 compounds in supercritical extracts of Beypazari lignite using deconvoluted
619 differential pulse polarograms, Energy Fuels 7 (1993) 620–624. Doi:
620 10.1021/ef00041a009
621 [34] D.M. Serafim, N.R. Stradiotto, Determination of sulfur compounds in gasoline using
622 mercury film electrode by square wave voltammetry, Fuel 87 (2008) 1007–1013. Doi:
623 10.1016/j.fuel.2007.07.012
624 [35] R. Joseph, K.G. Kumar, Differential pulse voltammetric determination and catalytic
625 oxidation of sulfamethoxazole using [5,10,15,20-tetrakis (3-methoxy-4-hydroxy
626 phenyl) porphyrinato] Cu (II) modified carbon paste sensor, Drug Test Anal. 2 (2010)
627 278–283. Doi: 10.1002/dta.129
628 [36] A.M. Oliveira Brett, L.A. da Silva, H. Fujii, S. Mataka, T. Thiemann, Detection of the
629 damage caused to DNA by a thiophene-S-oxide using an electrochemical DNA-
630 biosensor, J. Electroanal. Chem. 549 (2003) 91–99. Doi: 10.1016/S0022-
631 0728(03)00245-6
632 [37] I. Sirés, E. Brillas, Remediation of water pollution caused by pharmaceutical residues
633 based on electrochemical separation and degradation technologies: a review, Environ.
634 Int. 40 (2012) 212–229. Doi: 10.1016/j.envint.2011.07.012
635 [38] E. Brillas, C.A. Martínez-Huitle, Decontamination of wastewaters containing synthetic
636 organic dyes by electrochemical methods. An updated review, Appl. Catal. B: Environ.
637 166-167 (2015) 603–643. Doi: 10.1016/j.apcatb.2014.11.016

[39] A. Galia, S. Lanzalaco, M.A. Sabatino, C. Dispenza, O. Scialdone, I. Sirés, Crosslinking of poly(vinylpyrrolidone) activated by electrogenerated hydroxyl radicals: A first step towards a simple and cheap synthetic route of nanogel vectors, Electrochem. Commun. 62 (2016) 64–68. Doi: 10.1016/j.elecom.2015.12.005

[40] R. Trouillon, Y. Einaga, M.A.M. Gijs, Cathodic pretreatment improves the resistance of boron-doped diamond electrodes to dopamine fouling, Electrochem. Commun. 47 (2014) 92–95. Doi: 10.1016/j.elecom.2014.07.028

[41] K. Siuzdak, M. Ficek, M. Sobaszek, J. Ryl, M. Gnyba, P.N. Kowski, N. Malinowska, J. Karczewski, R. Bogdanowicz, Boron enhanced growth of micron-length carbon based nanowalls: a route towards high rates electrochemical biosensing, ACS Appl. Mater. Interfaces 9 (2017) 12982–12992. Doi: 10.1021/acsami.6b16860

[42] M. Madej, J. Kochana, B. Baś, Determination of viloxazine by differential pulse voltammetry with boron‑doped diamond electrode, Monats. Chem. 150 (2019) 1655–1665. Doi: 10.1007/s00706-019-2380-6

[43] K. Pecková, J. Musilová, J. Barek, Boron-doped diamond film electrodes-New tool for voltammetric determination of organic substances, Crit. Rev. Anal. Chem. 39 (2009) 148–172. Doi: 10.1080/10408340903011812

[44] T. Kondo, Y. Kodama, S. Ikezoe, K. Yajima, T. Aikawa, M. Yuasa, Porous boron-doped diamond electrodes fabricated via two-step thermal treatment, Carbon 77 (2014) 783–789. Doi: 10.1016/j.carbon.2014.05.082

[45] Y. Li, H. Li, M. Li, C. Li, D. Sun, B. Yang, Porous boron-doped diamond electrode for detection of dopamine and pyridoxine in human serum, Electrochim. Acta 258 (2017) 744–753. Doi: 10.1016/j.electacta.2017.11.121

[46] G. Bontempelli, F. Magno, G.A. Mazzocchin, S. Zecchin, Cyclic and a.c. voltammetric study on dibenzothiophene in acetonitrile medium, J. Electroanal. Chem. Interf. Electrochem. 43 (1973) 377–385. Doi: 10.1016/S0022-0728(73)80278-5

[47] E. Méndez-Albores, M.A. González-Fuentes, M.M. Dávila-Jiménez, F.J. González, Role of water in the formation of sulfoxide and sulfone derivatives during the electrochemical oxidation of dibenzothiophene in acetonitrile, J. Electroanal. Chem. 751 (2015) 7–14. Doi: 10.1016/j.jelechem.2015.05.025

[48] S. Shobal, Owolabi, M. Bankole, A.S. Ogunlaja, Electrochemical determination of trace sulfur containing compounds in model fuel based on silver/polyaniline-modified electrode, Anal. Methods 12 (2020) 1094–1106. Doi: 10.1039/C9AY02382H

[49] O. Ornelas Dávila, L. Lacalle Bergeron, P. Ruiz Gutiérrez, M.M. Dávila Jiménez, I. Sirés, E. Brillas, A.F. Roig Navarro, J. Beltrán Arandes, J.V. Sancho Llopis, Electrochemical oxidation of dibenzothiophene compounds on BDD electrode in acetonitrile–water medium, J. Electroanal. Chem. 847 (2019) 113172. Doi: 10.1016/j.jelechem.2019.05.054

[50] P.T. Cottrell, C.K. Mann, Electrochemical oxidation of aliphatic sulfides under nonaqueous conditions, J. Electrochem. Soc. 116 (1969) 1499–1503. Doi: 10.1149/1.2411587

[51] J. Iniesta, H. Alcock, D.J. Walton, M. Watanabe, S. Mataka, T. Thiemann, Electrochemical oxidation of tetracyclones and tetraphenylthiophene-S-oxide, Electrochim. Acta 51 (2006) 5682–5690. Doi: 10.1016/j.electacta.2006.03.001

[52] R.S. Nicholson, I. Shain, Theory of stationary electrode polarography. Single scan and cyclic methods, applied to reversible, irreversible, and kinetic systems, Anal. Chem. 36 (1964) 706–723. Doi: 10.1021/ac60210a007

[53] A.J. Bard, L.R. Faulkner, Electrochemical Methods Fundamentals and Application, 2nd ed., John Wiley, New York, 2001.

[54] F. Scholz, Electroanalytical Methods, 2nd ed., Springer, New York, 2005.

[55] A.J. Bard, L.R. Faulkner, Electrochemical methods, fundamentals and application, ed (John & Sons, Inc, New Jersey, 1980), p. 223E.

[56] D.P. Valencia, F.J. González, Estimation of diffusion coefficients by using a linear correlation between the diffusion coefficient and molecular weight, J. Electroanal. Chem. 681 (2012) 121–126. Doi10.1016/j.jelechem.2012.06.013

[57] P. Mericam. A. Astruc, M. Astruc, X. Andrieu, Contribution to the study of pulse polarography part III. Digital simulation of CE mechanisms in differential pulse polarography, J. Electroanal. Chem. Interf. Electrochem. 178 (1984) 235–245. Doi: 10.1016/S0022-0728(84)80003-0

[58] J. Wang, Analytical Electrochemistry, 2nd ed., Wiley-VCH, New York, 2000.

[59] T.E. Edmonds, The differential pulse polarographic determination of molybdenum in nitrate media, Anal. Chim. Acta 116 (1980) 323–333. Doi: 10.1016/S0003-2670(01)95212-2

[60] A. Deshpande, A. Bassi, A. Prakash, Ultrasound-assisted, base-catalyzed oxidation of 4,6-dimethyldibenzothiophene in a biphasic diesel-acetonitrile system, Energy Fuels 19 (2005) 28–34. Doi: 10.1021/ef0340965

[61] S. Matsuzawa, J. Tanaka, S. Sato, T. Ibusuki, Photocatalytic oxidation of dibenzothiophenes in acetonitrile using TiO_2: effect of hydrogen peroxide and ultrasound irradiation, J. Photochem. Photobiol A: Chem. 149 (2002) 183–189. Doi: 10.1016/S1010-6030(02)00004-7.

[62] J.D. Debad, J.C. Morris, P. Magnus, A.J. Bard, Anodic coupling of diphenylbenzo[*k*]fluoranthene: mechanistic and kinetic studies utilizing cyclic voltammetry and electrogenerated chemiluminescence, J. Org. Chem. 62 (1997) 530-537. Doi: 10.1021/jo961448e.

[63] M. Oyama, J. Matsui, Spectroscopic observation of the dimerization reactions of the 9-phenylcarbazole cation radical in acetonitrile, Bull. Chem. Soc. Jpn. 77 (2004) 953–957. Doi: 10.1246/bcsj.77.953.

[64] L. Eberson, M.P. Hartshorn, O. Persson, F. Radner, Redox and EPR spectral behaviour of radical cations of dibenzothiophene and some of its derivatives, Acta Chem. Scand. 51 (1997), 492-500. Doi: 10.3891/acta.chem.scand.51-0492.

718 **Figure captions**

719 **Fig. 1.** (a) CV and (b) DPV curves obtained in (---) 0.010 M $LiClO_4$ (background electrolyte)
720 dissolved in ACN and (a') in the same solution in the presence of 14 mg L^{-1} 4,6-DMDBT.
721 Anode: BDD; scan rate (v) = 0.003 V s^{-1}.

722 **Fig. 2.** Effect of experimental variables on the DPV profiles recorded on a BDD anode at ν
723 = 0.003 V s^{-1}. (a) Oxidation signals using (---) 0.010 M $LiClO_4$ in ACN, and in the presence
724 of 4,6-DMDBT at a concentration of: (a') 14 mg L^{-1}, (b') 7.0 mg L^{-1}, (c') 4.5 mg L^{-1}, (d') 3.0
725 mg L^{-1} and (e') 1.5 mg L^{-1}. The inset panel presents the corresponding peak current (I_p for
726 peak I) vs. 4,6-DMDBT content. (b) Oxidation of 14 mg L^{-1} 4,6-DMDBT in (a'') pure ACN
727 with 0.010 M $LiClO_4$, and in mixtures with an added water volume of: (b'') 50, (c´´) 100,
728 (d´´) 200, (e´´) 500 and (f'') 1000 μL. (c) Dependence of the peak current for peaks I and II
729 with the added water volume for the trials of plot (b). (d) Oxidation signals using (----) 0.010
730 M $LiClO_4$ in ACN (93.5% v/v)–water (6.5% v/v), and in the presence of 4,6-DMDBT at a
731 concentration of: (a') 27 mg L^{-1}, (b') 21 mg L^{-1} and (c') 14 mg L^{-1}. The inset panel shows the
732 change of the peak current for peaks I and II vs. 4,6-DMDBT content.

733 **Fig. 3.** (a) Influence of the scan rate on the cyclic voltammograms recorded in ACN (93.5%
734 v/v)–water (6.5% v/v, 0.010 M $LiClO_4$) using a BDD anode. (---) Oxidation without 4,6-
735 DMDBT at v = 0.003 V s^{-1}, and with 14 mg L^{-1} of this compound at v values of: (a') 0.100
736 V s^{-1}, (b') 0.075 V s^{-1}, (c') 0.050 V s^{-1}, (d') 0.025 V s^{-1}, (e') 0.010 V s^{-1} and (f') 0.005 V s^{-1}.
737 The inset panel depicts the change of the peak current for peak I with the square root of v, as
738 well as log I_p (for peak I) vs. log v. (b) Linear sweep voltammogram using the solution with
739 14 mg L^{-1} 4,6-DMDBT, at v = 0.005 V s^{-1}, subtracting the background current. The inset
740 panel presents the corresponding Tafel plot.

741 **Fig. 4.** (a) Same as plot 3a, but using the DPV technique. In the inset panel, dependence of
742 the peak current from peak I vs. *v*, as well as log *I* vs. log *v*. (b) Influence of 4,6-DMDBT
743 content on the DPV curves recorded under the same conditions at v = 0.003 V s^{-1}. (---)
744 Without 4,6-DMDBT, and in the presence of this compound at a content of: (a') 92 µM, (b´)
745 80 µM, (c´) 67 µM, (d´), 61 µM, (e´) 54 µM, (f´) 48 µM, (g´) 41 µM, (h´) 35 µM, (i') 28 µM,
746 (j') 21 µM, (k´) 14 µM and (l´) 7 µM. The inset panel presents the change of the peak current
747 for peak I vs. 4,6-DMDBT content.

748 **Fig. 5.** Suggested reaction mechanism for the electro-oxidation of 4,6-DMDBT in
749 acetonitrile–water medium using a BDD anode.

750 **Fig. 6.** DPV curves recorded at v = 0.003 V s^{-1} after the electrolysis of 27 mg L^{-1} 4,6-DMDBT
751 in ACN (93.5% v/v)–water (6.5% v/v, 0.010 M $LiClO_4$) in a BDD/BDD cell at an anodic
752 potential of 1.50 V. (a) After short electrolysis times: (a') initial, (b') 5 min, (c') 10 min, (d')
753 20 min, (e') 30 min, (f') 40 min, (g') 50 min and (h') 60 min. (b) After long electrolysis
754 times: (a´) initial, (b') 30 min, (c´) 60 min, (d´) 90 min. (e´) 120 min, (f´) 150 min, (g´) 180
755 min, (h´) 210 min and (i') 240 min. The inset panels of both graphs show the time course of
756 the normalized peak current for peak I and II at anodic potentials of (■) 1.50 and (●) 2.05
757 V, respectively.

758 **Fig. 7.** (a) Total ion chromatogram recorded by HPLC-UV (detection at λ = 232 nm) after 4
759 min of electrolysis under the same conditions of Fig. 10. The inset panel presents the time
760 course of the normalized area of peaks appearing at retention time of (■) 5.55 and (●) 10.81
761 min. (b) Percentage of conversion of 4,6-DMDBT to sulfoxide at a potential of 1.50 V during
762 the 90 min of electrolysis and pseudo-first-order kinetic analysis for the decay of 4,6-
763 DMDBT concentration.

764 **Fig. 8.** Chromatograms obtained by GC-MS analysis for samples collected at: (a') 0 min, (b')
765 15 min, (c') 30 min and (d') 60 min of electrolysis of 27 mg L^{-1} 4,6-DMDBT in ACN (93.5%
766 v/v)–water (6.5% v/v, 0.010 M $LiClO_4$) in a BDD/BDD cell at an anodic potential of 1.50 V.
767 The inset panel shows the normalized area vs. time for the two peaks detected. (b) Mass
768 spectrum of 4,6-DMDBT detected at retention time of 17.86 min. (c) Mass spectrum of 4,6-
769 DMDBTO detected at retention time of 20.24 min.

770 **Fig. 9.** Route proposed for the oxidation of 27 mg L^{-1} 4,6-DMDBT, including dimerization
771 and dimer oxidation upon bulk electrolysis for 90 min at 1.5 V. The products of the extract
772 were separated and analyzed by the UHPLC-ESI-Q-TOF-MS technique. Various arrows
773 indicate two or more successive reactions.

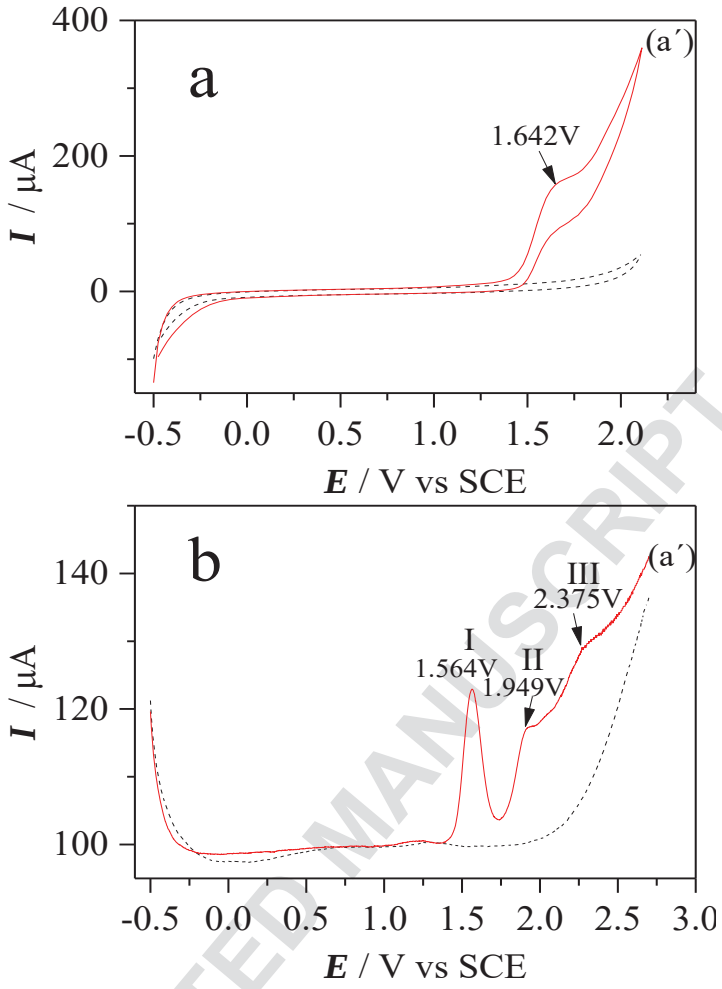

Fig. 1

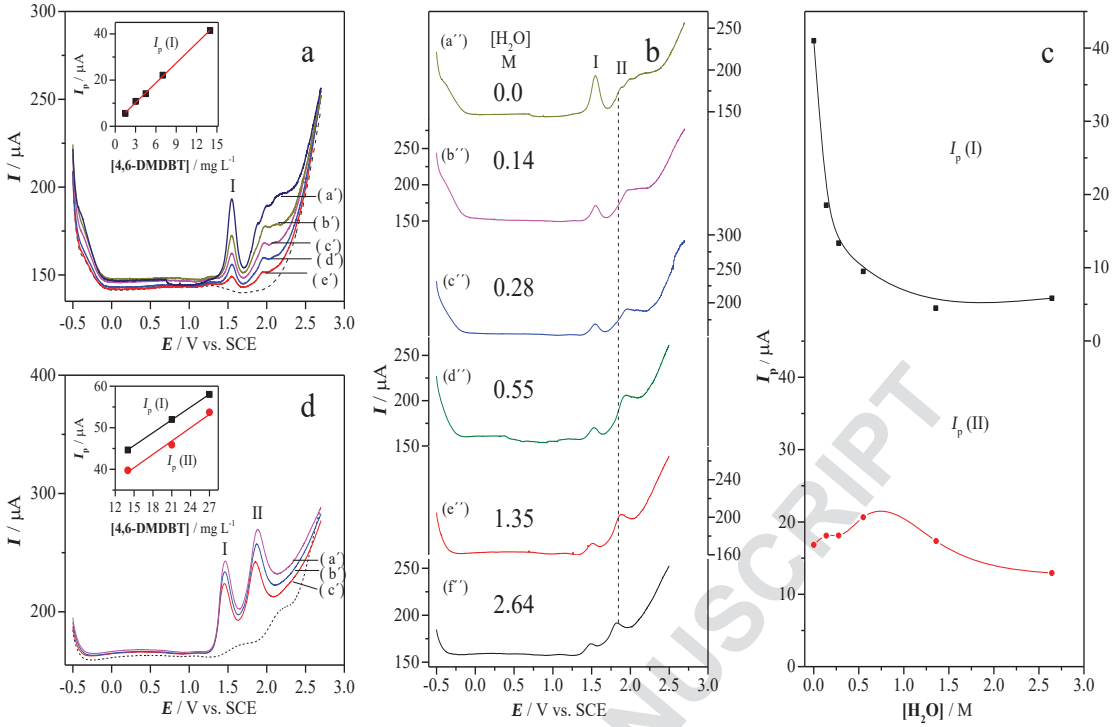

Fig. 2

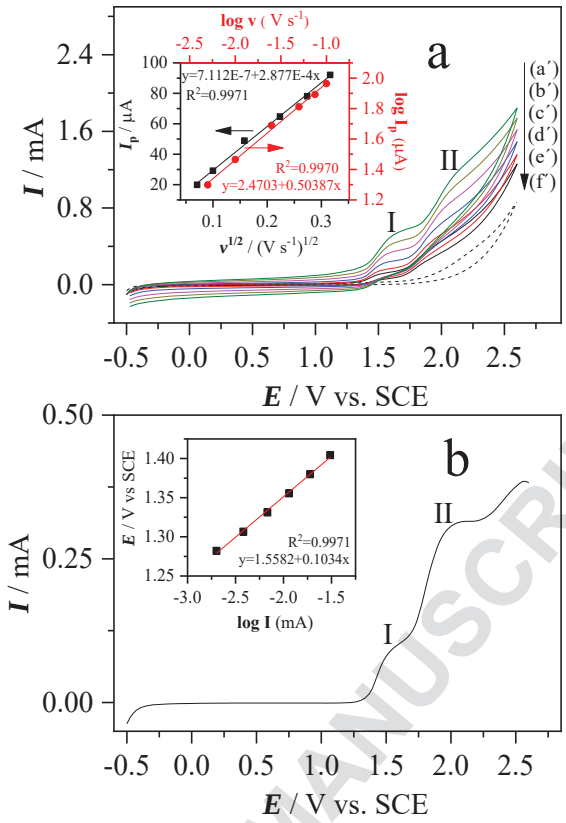

Fig. 3

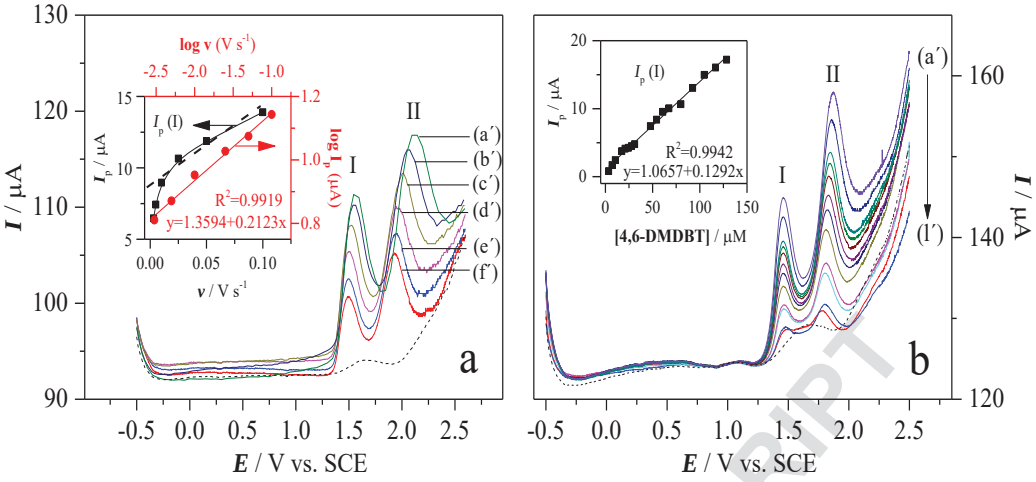

Fig. 4

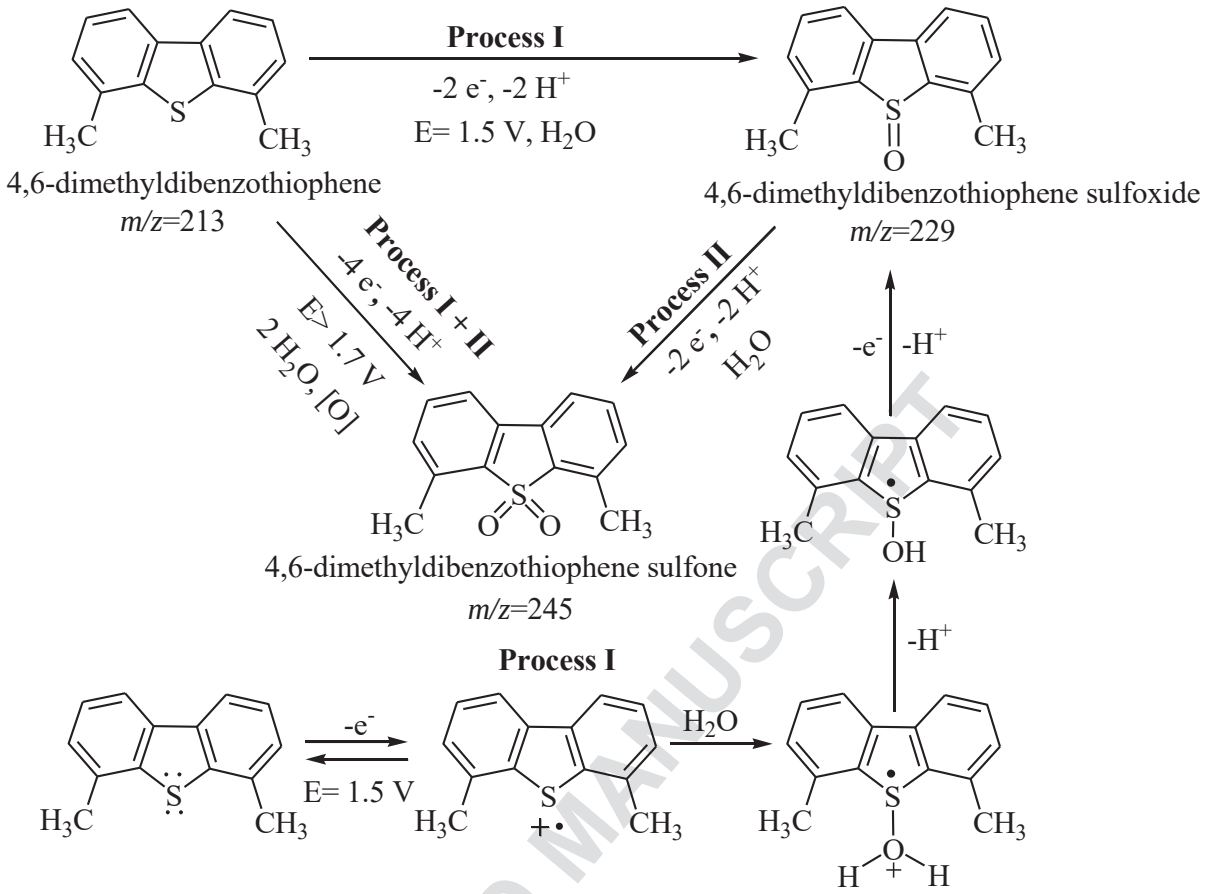

Fig. 5

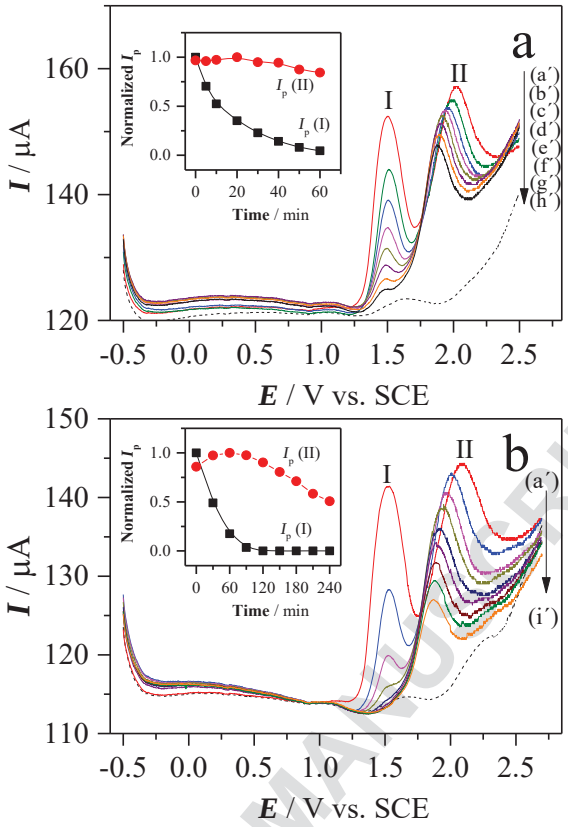

Fig. 6

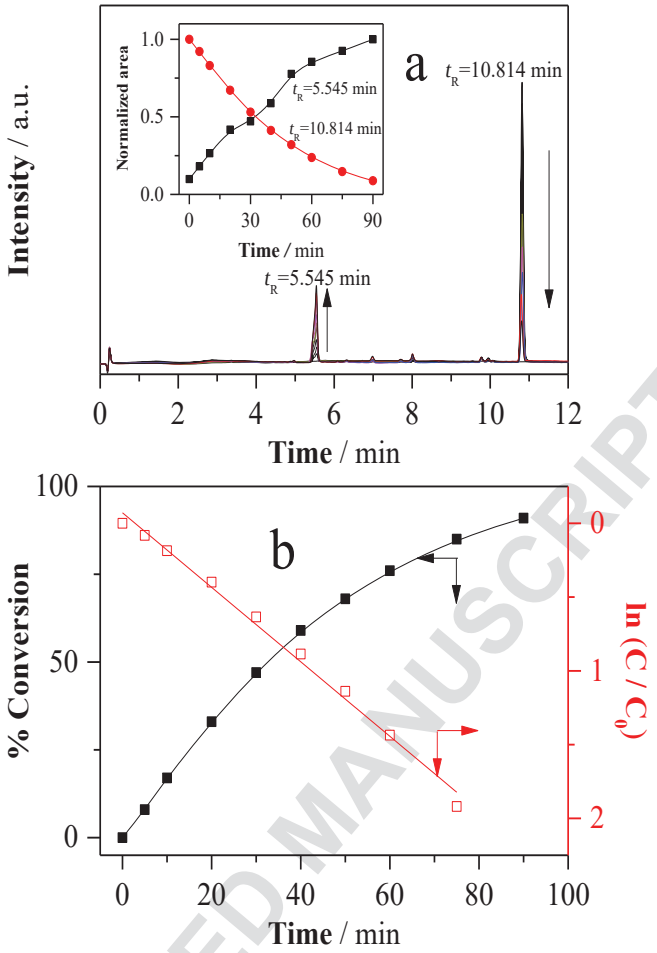

Fig. 7

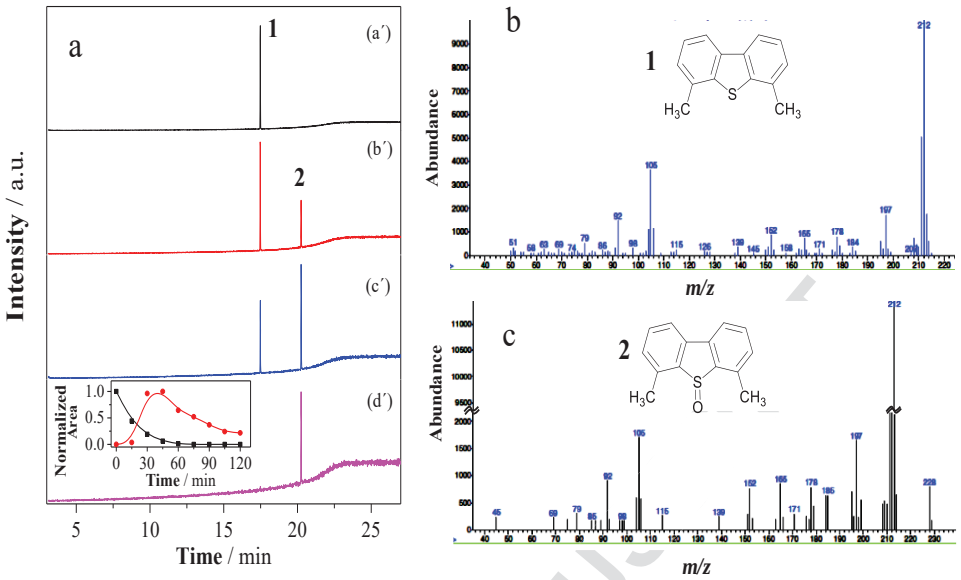

Fig. 8

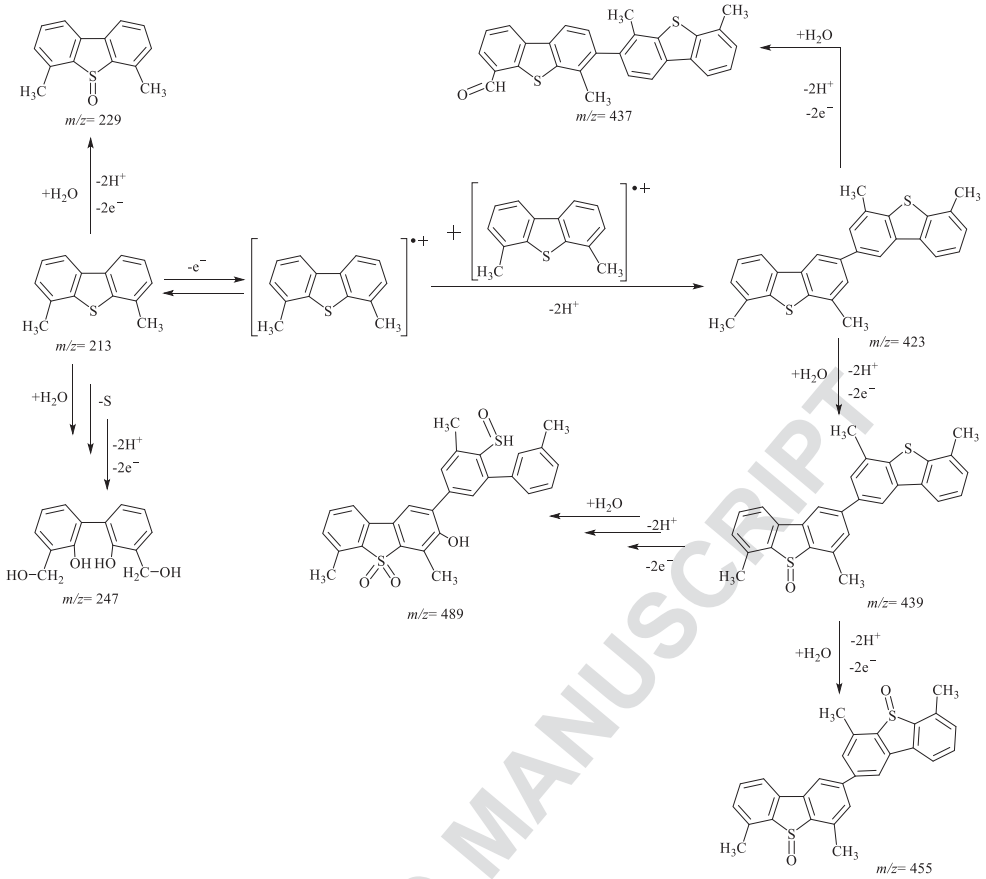

Fig. 9